Robert SURUS, Łukasz NIEWIARA, Tomasz TARCZEWSKI

Nicolaus Copernicus University in Torun, Insitute of Engineering and Technology

doi:10.15199/48.2023.05.42

A computationally efficient finite control set model predictive current control for reluctance synchronous motor

Abstract. *The paper presents a computationally efficient finite control set model predictive current control (FCS-MPC) for reluctance synchronous motor (RSM). Non-linear characteristics of d-q inductances have been applied to obtain an accurate model of the machine. These were used to calculate the maximum torque per ampere (MTPA) strategy. The reduction of the computational effort is obtained by decreasing the number of considered voltage vectors during selection. Extensive and accurate simulation studies indicate high-performance operation and torque ripple reduction of the drive.*

Streszczenie. *W artykule przedstawiono sterowanie predykcyjne prądami synchronicznego silnika reluktancyjnego charakteryzujące się zredukowaną złożonością obliczeniową. W układzie regulacji zaimplementowano strategię sterowania maksymalizującą rozwijany przez silnik moment elektromagnetyczny oraz szczegółowy model matematyczny uwzględniający zmienne indukcyjności w funkcji prądów. Zmniejszenie złożoności obliczeniowej uzyskano przez ograniczenie liczby wektorów stosowanych w procesie wyznaczania optymalnego sterowania. Wyniki badań symulacyjnych wykazały wysoką jakość pracy napędu oraz redukcję tętnień momentu elektromagnetycznego.* ***(Wydajne obliczeniowo sterowanie predykcyjne prądami synchronicznego silnika reluktancyjnego)***

Keywords: Finite Control Set, Model Predictive Currents Control, Reluctance Synchronous Motor, Time Horizon, Torque Ripple
Słowa kluczowe: Skończony Zbiór Sterowania, Sterowanie Predykcyjne Prądami, Synchroniczny Silnik Reluktancyjny, Horyzont Czasowy, Tętnienia Momentu

Introduction

The service life of AC motors is important for industrial devices. Their advantage is high energy efficiency. We distinguish between permanent magnet synchronous motors (PMSM), induction motors (IM), and reluctance motors. The main advantages of reluctance synchronous motor (RSM) are low vibration, higher energy efficiency [1, 2], and lower price due to the lack of the need for permanent magnets compared to PMSM and induction motors [3, 4]. RSMs can be used in electric vehicles [5], in HVAC applications [1], and in elevators [6].

The construction of the RSM is responsible for a variable inductance on the motor windings. Since the motor inductances depend on the current values, precise speed and torque control requires an accurate mathematical model [7]. Because of the similarity in the principle operation of RSM, PMSM, and IM, a cascade control structure with field oriented control strategy can be used [7]. The main disadvantage of this solution is related to low dynamics of speed control loop. As an alternative to the standard cascade control structure, a state feedback controller [8, 9], the sliding mode controller [10], H_∞ control [11], and model predictive control [12, 13] can be used. Due to high-performance, quick response and simple computation, the finite control set model predictive control (FCS-MPC) seems to be a promising approach for RSM. Here, values of the control signals are obtained during optimization procedure where specific cost function is minimized. In the result, the optimal voltage vector is determined for a specific time horizon and used in switching the inverters' transistors. Considered control structure operates without space vector modulator and with limited number of parameters when compared to field oriented control structure. Since FCS-MPC has been firstly adopted to control PMSM and IM, it is often assumed that the value of the inductances is constant. Such a solution is not suitable for RSM since it may result in a poor current control performance due to electrical time constant mismatch [12]. Moreover, considered inconsistency will increase the torque ripples and decrease the control performance due to possible vibrations and acoustic noise [14]. Besides this, the efficient torque generation requires application of suitable control strategy, i.e., the maximum torque per ampere (MTPA) and/or the maximum torque per voltage (MTPV) [15]. In the case of FCS-MPC, the time horizon is an important parameter that impacts the control performance and the computational complexity. For that reason, its value should be selected carefully, taking into account aforementioned requirements and hardware capabilities.

Conventional FCS-MPC is characterized by high computational complexity. As the time horizon increases, the number of possible voltage vectors and cost functions that are optimized increases exponentially [16]. For industrial systems with low computing power, it is necessary to simplify the control algorithm. To simplify the complexity of the algorithm strategy to use an adding judgment [17] or the combination of constraints such as torque error, flux linkage position and flux linkage error [16] or adding a penalty overcurrent term in the cost function can be used [18].

In this paper, the computationally efficient finite set control and model predictive currents control are proposed. The simplification consists in reducing the number of voltage vectors during selection. The selection of the voltage vectors from vectors with only even or only odd indices was proposed. The impact of the time horizon for torque ripples for reluctance synchronous motor with conventional and computationally efficient finite set control and model predictive currents control is researched. The speed control is made using PI controller and the maximum torque per ampere (MTPA) strategy. Extensive and accurate simulation studies were conducted in the Matlab/Simulink and the PLECS environment.

Mathematical model of drive

In most cases, the RSM control is realized in a rotating reference frame (RRF) coordinate system, which requires the mathematical model to be defined as D- and Q-axis components of flux linkage and current. In respect to the above, the mentioned model can be represented by the following equations:

$$\frac{d\psi_d(t)}{dt} = u_d(t) - Ri_d(t) + n_p\omega_m(t)\psi_q(t) \tag{1}$$

$$\frac{d\psi_q(t)}{dt} = u_q(t) - Ri_q(t) - n_p\omega_m(t)\psi_d(t) \tag{2}$$

$$J\frac{d\omega_m(t)}{dt} = \frac{3}{2}n_p(\psi_d(t)i_q(t) - \psi_q(t)i_d(t)) - B\omega_m(t) - T_L(t) \tag{3}$$

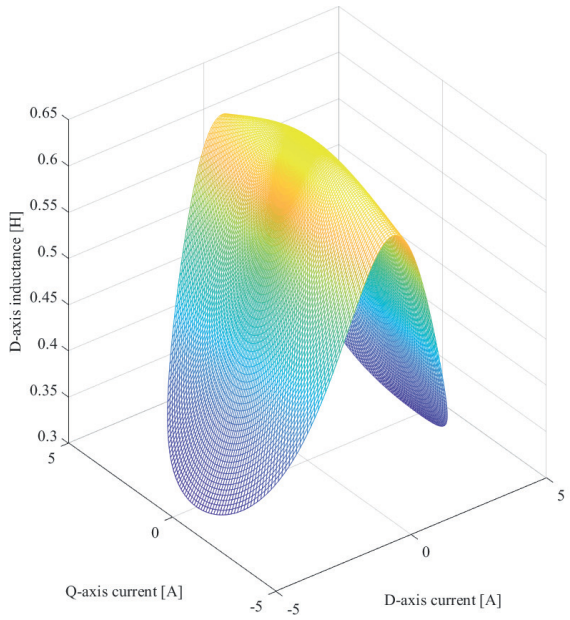

Fig. 1. The determined characteristics of D- and Q-axis inductance

$$\psi_d(t) = L_d\Big(i_d(t), i_q(t)\Big) i_d(t) \tag{4}$$

$$\psi_q(t) = L_q\Big(i_d(t), i_q(t)\Big) i_q(t) \tag{5}$$

where: $u_d(t)$ and $u_q(t)$ - input voltages given in RRF, $i_d(t)$ and $i_q(t)$ - stator current components given in RRF, $\psi_d(t)$ and $\psi_q(t)$ - magnetic flux components, R - stator resistance, n_p - number of pole pairs, $\omega_m(t)$ - angular velocity of the rotor, J - moment of inertia, B - viscous friction coefficient, and $T_L(t)$ - external load torque.

Since the magnetic saturation phenomenon occurs, the D- and Q-axis components of the inductance are strongly non-linear and current dependent. The assumed characteristics of $L_d(i_d, i_q)$ and $L_q(i_d, i_q)$ are presented on Fig. 1. The source of the inductance characteristics is experimental identification by indirectly measuring the magnetic flux. The equations for L_d and L_q are written as [19]:

$$L_d(i_d, i_q) = L_{d0}(i_d) - L_{d1}(i_d) L_{q2}(i_q) \tag{6}$$

$$L_q(i_d, i_q) = L_{q0}(i_q) - L_{q1}(i_q) L_{d2}(i_d) \tag{7}$$

with:

$$L_{d0}(i_d) = A_0 + \frac{B_0}{i_d^4 + C_0 i_d^2 + D_0} \tag{8}$$

$$L_{d1}(i_d) = \frac{B_1}{i_d^4 + C_1 i_d^2 + D_1} \tag{9}$$

$$L_{q2}(i_q) = 1 - \frac{1}{C_q i_q^2 + 1} \tag{10}$$

$$L_{q0}(i_q) = A_2 + \frac{B_2}{i_q^4 + C_2 i_q^2 + D_2} \tag{11}$$

$$L_{q1}(i_q) = \frac{B_3}{i_q^4 + C_3 i_q^2 + D_3} \tag{12}$$

$$L_{d2}(i_d) = 1 - \frac{1}{C_d i_d^2 + 1} \tag{13}$$

where: A_0, B_0, C_0, D_0, A_1, B_1, C_1, D_1 and C_q are the constant coefficients in $L_d(i_d, i_q)$, while A_2, B_2, C_2, D_2, A_3, B_3, C_3, D_3 and C_d are the constant coefficients in $L_q(i_d, i_q)$. Values of the inductance coefficients were determined by indirect measurement of the magnetic flux for different values of the current components and the polynomial approximation in the Matlab environment. These are presented in Table 1. As it was stated in [16] proper prediction of current components requires complex model including the non-linear characteristics of motor inductance.

Table 1. Values of constants for the approximation of inductance

A_0	B_0	C_0	D_0
0.147	5039	1317	9538
B_1	C_1	D_1	C_q
1379	684.2	10237	0.024
A_2	B_2	C_2	D_2
0.093	45731	386480	221393
B_3	C_3	D_3	C_d
595615	64498	7068634	0.035

Control Structure

The control structure is a cascade connection of PI velocity controller, MTPA strategy and model predictive current control (MPCC) structures. The overall block diagram of the control structure is presented in Fig. 2. The determined MTPA trajectory based on the assumed inductance characteristics is shown in Fig. 3. First of all, the current controller should be developed in respect to the assumed non-linear model of the plant. Therefore, an appropriate cost function and a corresponding discrete prediction model of the current loop should be prepared. The model predictive current controller the following cost function as the control quality indicator was adopted:

$$g_{0,\dots,7} = \sum_{n=1}^{N} \Big(\Big(i_{sd}^{ref}(k+n) - i_{sd}^{p}(k+n) \Big)^2 + \Big(i_{sq}^{ref}(k+n) - i_{sq}^{p}(k+n) \Big)^2 \Big) \tag{14}$$

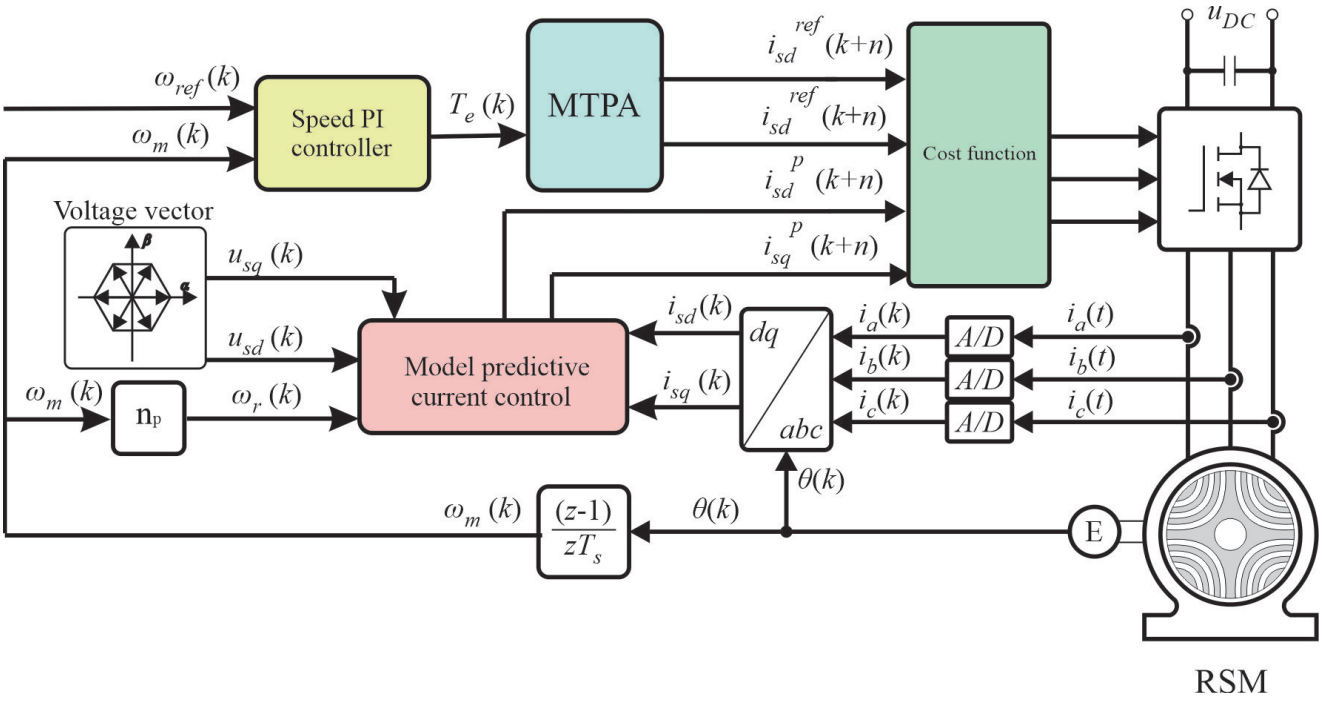

Fig. 2. Block diagram of the PI-MTPA-MPCC control structure for Reluctance synchronous motor

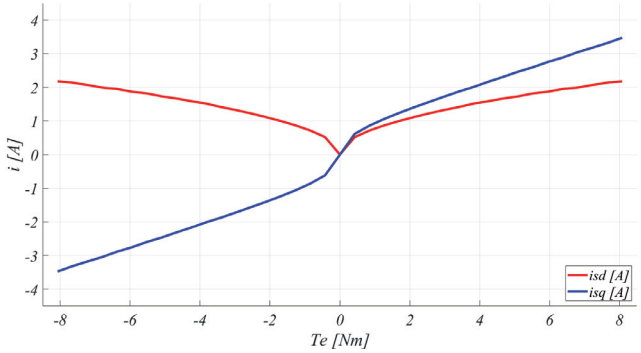

Fig. 3. The determined MTPA trajectory - current components i_{sd} and i_{sq} in function of torque

where: $g_{0,\dots,7}$ - the cost function, $i_{sd}^{ref}(k+n)$ and $i_{sq}^{ref}(k+n)$ - reference rotor and stator current components in next moment of time, $i_{sd}^{p}(k+n)$ and $i_{sq}^{p}(k+n)$ - predicted rotor and stator current components in next moment of time, $u_{0,\dots,7}$ - the vector of voltage, N - the prediction horizon.

Values of the presented cost function are subject to the minimization process. For the minimized cost function, appropriate voltage vectors were determined. Each of them is directly related to a corresponding state of the switches in the power stage. The discrete current-prediction model may be obtained using Euler discretization method applied to the mathematical model given by formulas (1)–(5). The predicted current value for the next sampling period can be calculated on the basis of the relationships given below:

$$i_{sd}^{p}(k+1) = \Big(1 - \frac{T_s R}{L_d(i_{sd}(k), i_{sq}(k))}\Big) i_{sd}(k) + \\ + T_s \xi(k) \omega(k) i_{sq}(k) + \frac{T_s u_{sd}(k)}{L_d(i_{sd}(k), i_{sq}(k))} \tag{15}$$

$$i_{sq}^{p}(k+1) = \Big(1 - \frac{T_s R}{L_q(i_{sd}(k), i_{sq}(k))}\Big) i_{sq}(k) + \\ + T_s \xi(k)^{-1} \omega(k) i_{sd}(k) + \frac{T_s u_{sq}(k)}{L_q(i_{sd}(k), i_{sq}(k))} \tag{16}$$

with:

$$\xi(k) = \frac{L_q(i_{sd}(k), i_{sq}(k))}{L_d(i_{sd}(k), i_{sq}(k))} \tag{17}$$

where: T_s is a sampling period, $i_{sd}(k)$ and $i_{sq}(k)$ - measured stator and rotor current values [12]. It should be noted that the assumed model takes into account the non-linear behavior of inductance components on both axes.

Since the rotor excitation is strictly related to the D-axis current component, the torque produced by the motor should be optimized in respect to the value of stator current. Therefore in the second step of controller synthesis, the MTPA strategy should be developed in order to optimize the efficiency of the drive system. The considered motor does not have any magnets in its structure, therefore the phase of optimal current angle varies with the demanded value of torque.

Finally, after the development of MPCC and MTPA strategies, the velocity controller may be designed. A classical PI controller is employed for angular velocity regulation. The output signal of the velocity controller sets the demand torque for the MTPA-MPCC block. The PI speed controller parameters were selected using the Ziegler-Nichols second criterion.

Computationally efficient FCS-MPC

In conventional MPCC, seven different voltage vectors are used in each prediction step. The different eight switching states of the inverter designated as $u_0 \div u_7$ and the corresponding voltage vectors in stationary reference frame $\alpha\,\beta$ are listed in table 2 and Fig. 5. Then, Park transformation is provided to convert the stator voltages into rotating frame dq.

The dependence between the prediction horizon and the number of possible cost functions is an exponential one. For a conventional MPCC we get the following relationship:

$$m = 7^N \tag{18}$$

where m is the number of possible cost function values and N is the prediction horizon. The dependence (18) for a

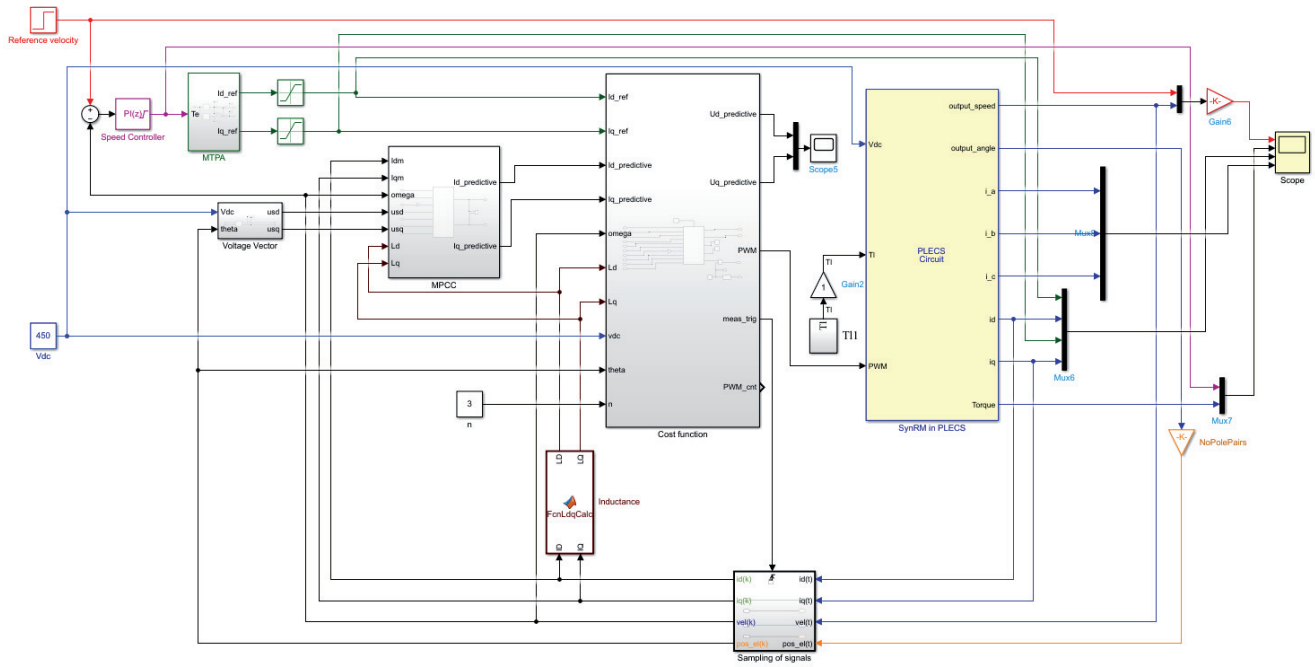

Fig. 4. The block structure of control system with MPCC and MTPA in MATLAB/Simulink enviroment

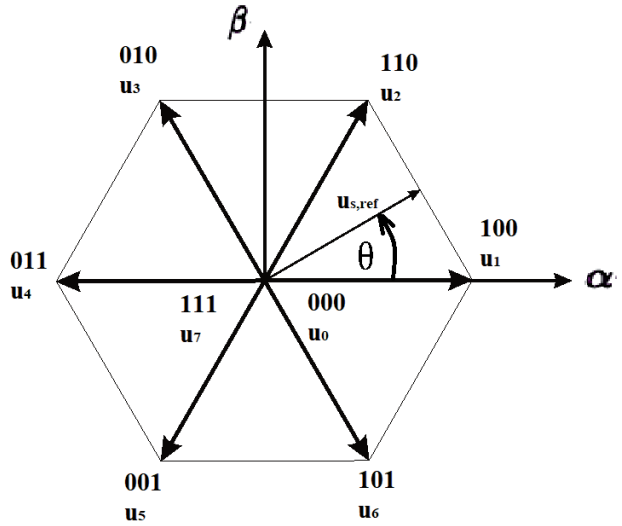

Fig. 5. Voltage vectors in conventional MPCC

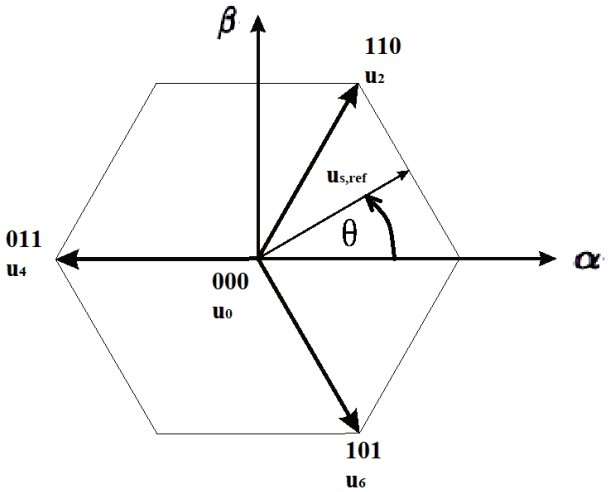

Fig. 6. Voltage vectors in computationally efficient MPCC with only vectors with even indices

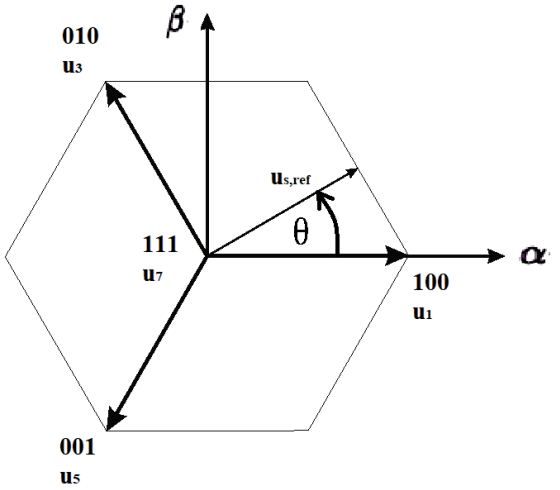

Fig. 7. Voltage vectors in computationally efficient MPCC with only vectors with odd indices

Table 2. Voltage vectors for conventional MPCC

Conducting modes	Switching states	Output Voltages
	$S_a\ S_b\ S_c$	V_α, V_β
u_0	0 0 0	$0, 0$
u_1	1 0 0	$\frac{2V_{dc}}{3}, 0$
u_2	1 1 0	$\frac{V_{dc}}{3}, \frac{\sqrt{3}V_{dc}}{3}$
u_3	0 1 0	$-\frac{V_{dc}}{3}, \frac{\sqrt{3}V_{dc}}{3}$
u_4	0 1 1	$\frac{V_{dc}}{3}, 0$
u_5	0 0 1	$-\frac{V_{dc}}{3}, -\frac{\sqrt{3}V_{dc}}{3}$
u_6	1 0 1	$\frac{V_{dc}}{3}, -\frac{\sqrt{3}V_{dc}}{3}$
u_7	1 1 1	$0, 0$

fixed prediction horizon (e.g. $N = 3$) clearly indicates that the number of voltage vectors used to determine the optimal control sequence has a significant impact on the computational complexity. A following simplification of MPCC, which can be used in systems with limited computing power was proposed. In order to reduce the computational complexity,

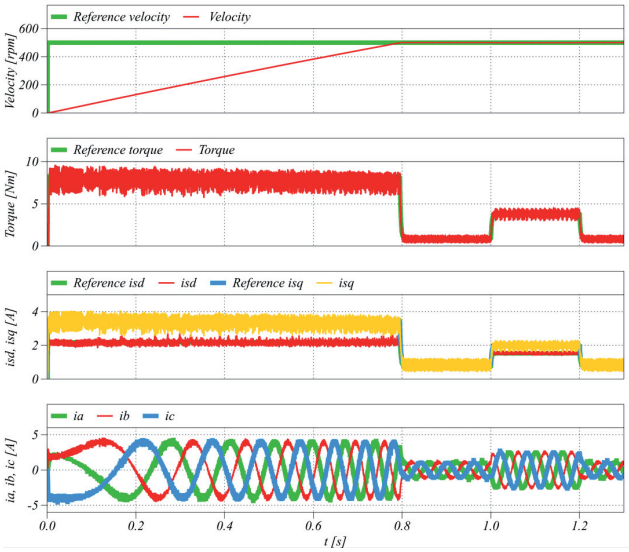

Fig. 8. Simulation results for velocity step response under load operation with conventional MPCC strategy for the prediction horizon equal to 1

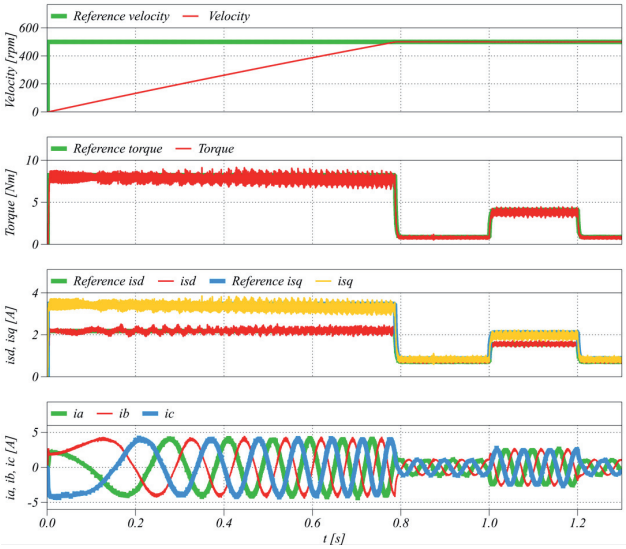

Fig. 9. Simulation results for velocity step response under load operation with conventional MPCC strategy for the prediction horizon equal to 3

it was decided to use only 4 vectors of voltages with even (u_0, u_2, u_4, u_6) or odd (u_1, u_3, u_5, u_7) indicies. The voltage vectors for computationally efficient MPCC is shown on the Fig. 6 and Fig. 7. The division was made in a way that ensures even coverage of the space visible in Fig. 5. The proposed solution reduces the computational complexity as follows:

$$m = 4^N \tag{19}$$

The described control strategy reduces the number of considered cost functions. In the result, proposed solution should be suitable for control systems with reduced computing power.

Simulation Results

The above-mentioned mathematical description of the RSM was applied to build a simulation model in the Matlab/Simulink environment, as shown in Fig. 4. In order to obtain more accurate simulation results the model of inverter and RSM was built in PLECS environment and it was presented in Fig. 10. The main parameters of the simulation tests are shown in table 3.

Table 3. Parameters of reluctance synchronous motor drive

Parameter name	Symbol	Value	Unit
DC-link voltage	U_{DC}	450	V
Sampling frequency	f_{sw}	10.0	kHz
Rated current (RMS)	I_N	2.9	A
Rated torque	T_N	7.0	Nm
Rated velocity	N_N	1500	rpm
Rated power	P_N	1.1	kW
Stator resistance	R_s	6.0	Ω
Number of pole pairs	n_p	2	-
Moment of inertia (summarized)	J	0.111	kgm^2
Viscous friction coefficient	B	0.015	Nms/rad

The reference value of currents in the RRF system were determined using the MTPA strategy based on the trajectories from Fig. 3. It was assumed that the D- and Q-axis inductance components are non-linearly dependent on the current-space vector components i_{sd} and i_{sq}, as shown in Fig. 1. The MTPA strategy based on relation between D- and

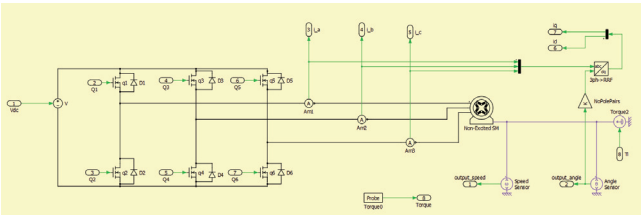

Fig. 10. The block structure of inverter and reluctance synchronous motor in PLECS environment

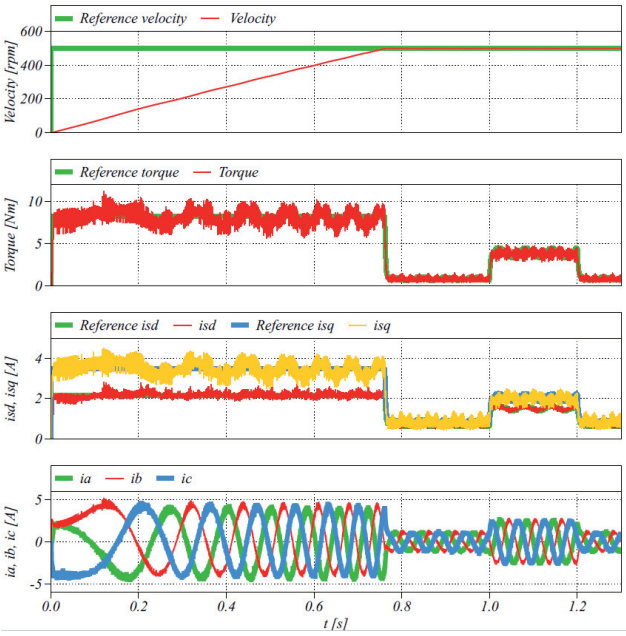

Fig. 11. Simulation results for velocity step response under load operation with proposed computationally efficient MPCC strategy for the prediction horizon equal to 1 and four voltage vectors with odd indices

Q-current components in function of torque (Fig. 3) has been implemented using one-dimensional look-up tables. Next, it was assumed that the proportional gain K_p of the PI speed controller is 55.5 and the integration time T_i is 0.056 s. The sampling period is 100 μs. A step of load torque equal to 3 Nm was imposed between 1 s and 1.2 s, respectively. The waveforms of rotational speed, torque, current-space vector

Table 4. Torque ripple amplitude range values for conventional FCS-MPC

Time horizon	Number of possible voltage vectors	Torque ripple amplitude range	Unit
1	7	3.81495	Nm
2	49	3.83218	Nm
3	343	2.59626	Nm
4	2401	3.72519	Nm
5	16807	2.60103	Nm

Table 5. Torque ripple amplitude range values for computationally efficient FCS-MPC

Time horizon	Number of possible voltage vectors	Torque ripple amplitude range - voltage vectors with odd indices	Torque ripple amplitude range - voltage vectors with even indices	Unit
1	4	5.52693	4.08071	Nm
2	16	5.51317	4.18261	Nm
3	64	3.26911	3.11164	Nm
4	256	5.52630	4.17291	Nm
5	1024	3.27812	3.13155	Nm

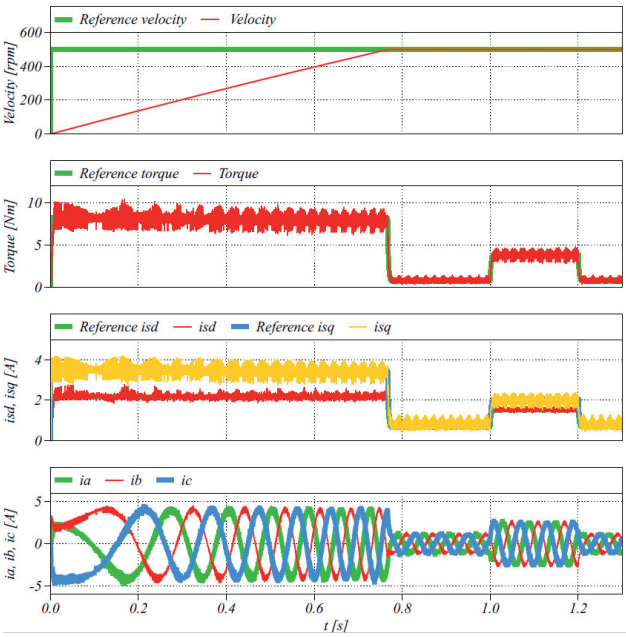

Fig. 12. Simulation results for velocity step response under load operation with proposed computationally efficient MPCC strategy for the prediction horizon equal to 1 and four voltage vectors with even indices

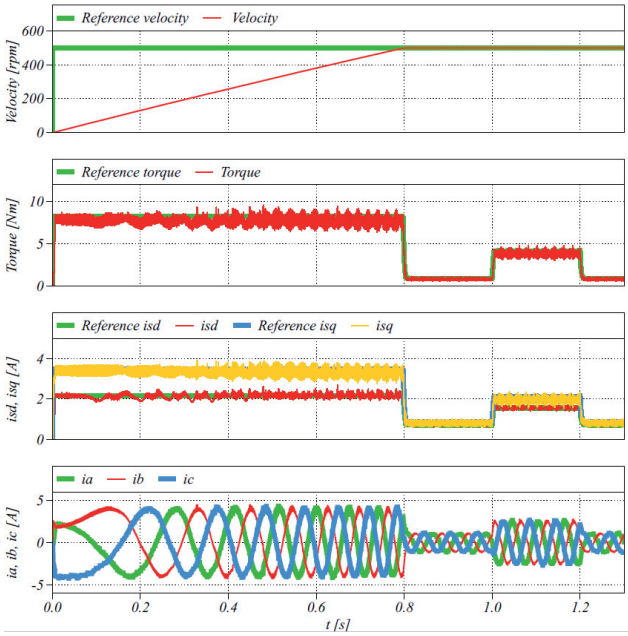

Fig. 13. Simulation results for velocity step response under load operation with proposed computationally efficient MPCC strategy for the prediction horizon equal to 3 and four voltage vectors with odd indices

components phase currents were presented in Fig. 8 and Fig. 9 for the control system with the proposed MPCC strategy taking into account the non-linear characteristics of inductance components for all voltage vectors and time horizons equal to 1 and 3. Fig. 11 and Fig. 13 shows the simulation results for MPCC structure based on a simplified model with only four voltage vectors with odd index. Fig. 12 and Fig. 14 shows the simulation results for MPCC structure based on a simplified model with only four voltage vectors with even index. The tests were carried out in the same way as for the nonlinear system. By analyzing the received waveforms, it can be concluded that the motor currents do not exceed their maximum value providing safe and efficient operation of RSM. During speed-up, the torque maintains its maximum value, which confirms the correct operation of the MTPA strategy. The use of a computationally efficient MPCC with four voltage vectors with even indices allows to obtain a range of torque ripple amplitude close to the conventional MPCC. The speed is maintained at a reference level, which confirms the correct operation of the conventional and the computationally efficient FCS-MPC.

Based on the obtained results, it can be stated that the for a conventional MPCC, the amplitude of torque ripple is at the level of 1.22 Nm. The use a computationally efficient MPCC with four voltage vectors with odd indices results in torque ripple equals to 2.25 Nm, while the model with four voltage vectors with even indices provides the torque ripple at the level of 1.07 Nm. In the case of the prediction horizon value, it was found that the best control performance is obtained for its value equal to 3. In the Fig. 15 the minimum values of the cost function for the consecutive registered samples is presented. From obtained results, it can be concluded that the proposed solution ensures proper operation of the RSM (i.e., reduced torque ripples) with limited computational complexity. Due to this further improvement of the control performance related to increased number of prediction horizon can be utilized in the drives with relative low computing power [20]. Obtained values of torque ripples in the function

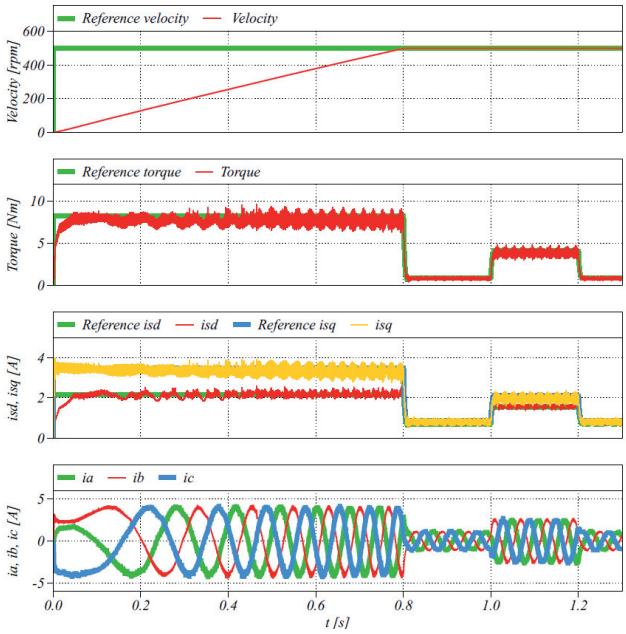

Fig. 14. Simulation results for velocity step response under load operation with proposed computationally efficient MPCC strategy for the prediction horizon equal to 3 and four voltage vectors with even indices

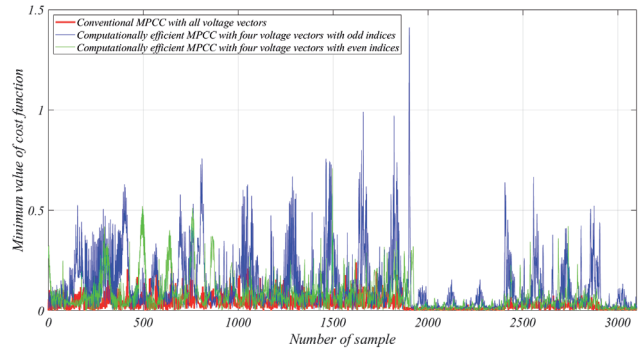

Fig. 15. Minimum cost function for conventional MPCC with all voltage vectors and proposed computationally efficient MPCC for the prediction horizon equal to 3

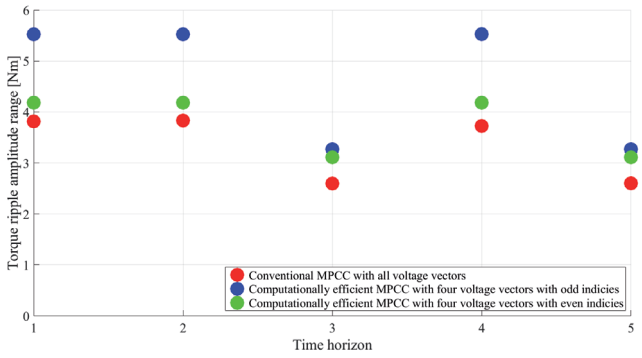

Fig. 16. The dependence between the torque ripples and the prediction horizon for conventional MPCC and computationally efficient MPCC

of the prediction horizon are summarized in tables 4, 5 and shown in the Fig. 16. For the time horizon equal to 3 and 5, the computationally efficient MPCC with four vectors with odd indices allows to obtain the range of the amplitude ripple of the torque close to the amplitude range of the torque ripple for the proposed conputationally efficient MPCC with four vectors with even indices.

Conclusion

In this paper, the computationally efficient finite control set model predictive current control for synchronous reluctance motor has been proposed. To maximize the efficiency of the motor, the MTPA control strategy has been implemented. Based on the conducted numerical experiments, the optimal prediction horizon length and the computationally efficient model has been proposed as a compromise between the drive performance and the computational complexity. It was found that proper operation of RSM drive can be obtained for MPCC with reduced number of voltage vectors. Experimental verification of the proposed solution is planned in the near future.

REFERENCES

[1] Oliveira F., Ukil A.: Comparative Performance Analysis of Induction and Synchronous Reluctance Motors in Chiller Systems for Energy Efficient Buildings IEEE Transactions on Industial Informatics, Vol. 15, No. 8, 2019

[2] Murataliyev M., M. Degano, M. Di Nardo, N. Bianchi, C. Gerada.: Synchronous Reluctance Machines: A Comprehensive Review and Technology Comparison, Proceedings of the IEEE, p. 382 - 399, 11 February 2022

[3] Im J. B., Kim W., Kim K., Jin C. S., Choi J. H., Lee J.: Inductance Calculation Method of Synchronous Reluctance Motor Including Iron Loss and Cross Magnetic Saturation, IEEE Transactions on Magnetics, Vol. 45, no. 6, 2009

[4] Niedworok A., Orzech Ł.: Assessment of efficiency of drive equipped with induction motor and drive equipped with reluctance motor, Przeglad Elektrotechniczny, ISSN 0033-2097, R. 92 NR 8/2016 (in Polish)

[5] Li J. C., Xin M., Fan Z. N., Liu R.: Design and Experimental Evaluation of a 12 kW Large Synchronous Reluctance Motor and Control System for Elevator Traction, IEEE Access,Vol. 8, 2020

[6] Lin F.J., Huang M.S., Chen S. G., Hsu C. W., Liang C. H.: Adaptive Backstepping Control for Synchronous Reluctance Motor Based on Intelligent Current Angle Control, IEEE Transactions on Power Electronics, Vol. 35, No. 7, 2020

[7] Boldea, I., Tutelea L.: Reluctance Electric Machines: Design and Control, CRC Press, 2018

[8] Tarczewski T., Niewiara Ł. J., Grzesiak L.: Gain-Scheduled State Feedback Speed Control of Synchronous Reluctance Motor, 2021 IEEE 19th International Power Electronics and Motion Control Conference (PEMC), 25-29 April 2021, Gliwice, Poland

[9] Awan H. A. A., Saarakkala S. E., Hinkkanen M.: Assessment of efficiency of drive equipped with induction motor and drive equipped with reluctance motor, Flux-Linkage-Based Current Control of Saturated Synchronous Motors, IEEE Transactions on Industry Application, Vol. 55, No. 5, 2019

[10] Zhang X., Sun L., Zhao K., Sun L.: Nonlinear Speed Control for PMSM System Using Sliding-Mode Control and Disturbance Compensation Techniques, IEEE Transactions on Power Electronics , Vol. 28, No. 3, 2013

[11] Bingyou L.: Research on H infinity Robust Tracking Controller for Permanent Magnet Synchronous Motor Servo System, 2009 International Conference on Information Engineering and Computer Science, 19-20 Dec. 2009, Wuhan, China

[12] Farhan A., Abdelrahem M., Saleh A., Shaltout A., Kennel R.: Simplified Sensorless Current Predictive Control of Synchronous Reluctance Motor Using Online Parameter Estimation, MDPI, Energies, 2020

[13] Miloud G., Hicham S., Youcef B.: Sensorless Speed Control of Synchronous Reluctance Motors Using Model Predictive control associated with Model Reference Adaptive System, 2021 IEEE 1st International Maghreb Meeting of the Conference on Sciences and Techniques of Automatic Control and Computer Engineering MI-STA, 2021

[14] Y. Yamamoto, S. Morimoto, M. Sanada, Y. Inoue.: Torque Ripple Reduction Using Asymmetric Flux Barriers in Synchronous Reluctance Motor, 2018 International Power Electronics Conference (IPEC-Niigata 2018 -ECCE Asia), Niigata, Japan

[15] H. Mahmoud, G. Bacco, M. Degano, N. Bianchi, C. Gerada.: Synchronous Reluctance Motor Iron Losses: Considering Machine Nonlinearity at MTPA, FW, and MTPV Operating Conditions, IEEE Transactions On Energy Conversion, Vol. 33, No.

3, September 2018
[16] Y. Li, Z. Liu, X. Wang, G. Chen, C. Ren, D. Liu.: Simplified Multi-Step Predictive Current Control for Surface Permanent Magnet Synchronous Motor The 6th IEEE International Conference on Predictive Control of Electrical Drives and Power Electronics, 2021
[17] Y. Li, X. Wang, Z. Liu, G. Chen, D. Liu, C. Ren.: Simplified Control Strategy for Permanent Magnet Synchronous Motor Model Predictive Torque Control The 6th IEEE International Conference on Predictive Control of Electrical Drives and Power Electronics, 2021
[18] Y. Li, Z. Liu, X. Wang, G. Chen, C. Ren, D. Liu.: Low-Complexity Finite Control Set Model Predictive Control With Current Limit for Linear Induction Machines IEEE Transactions On Industrial Electronics, Vol. 65, No. 12, December 2018
[19] S. Yamamoto, T. Ara, K. Matsuse.: A Method to Calculate Transient Characteristics of Synchronous Reluctance Motors Considering Iron Loss and Cross-Magnetic Saturation, IEEE Transactions on Industry Applications, Vol. 43, No. 1, 2007
[20] R. Surus, Ł. Niewiara, T. Tarczewski, L. M. Grzesiak.: Finite control set model predictive current control for reluctance synchronous motor, The 20th IEEE International Conference on Power Electronics And Motion Control, 2022